J Solid State Electrochem (2012) 16:1509–1517
DOI 10.1007/s10008-011-1554-x

ORIGINAL PAPER

Performance of planar electrode-supported high-temperature solid oxide fuel cell using syngas

Jianguo Yu · Xiuling Cao · Yuzhang Wang

Received: 5 July 2011 / Revised: 6 September 2011 / Accepted: 9 September 2011 / Published online: 2 October 2011

Abstract In China, coal is a dominant energy source. In order to ensure China's energy security, coal should be used efficiently and cleanly. Integrated gasification fuel cell hybrid power generation system is a promising system for coal utilization. It combines clean coal gasification technology with high efficient fuel cell technology. In this work, the performance of solid oxide fuel cell using syngas as fuel was investigated, based on the commercial computational fluid dynamic software and the developed program used to analyze chemical, electrochemical, heat/mass transfer, current, and electric potential. The results show that the temperature difference is about 300 K in the cell under all calculation conditions. Along the cell length, hydrogen concentration rapidly reduces, and its decrement is larger than that of carbon monoxide. The variation of current density in electrolyte layer is relatively small along the direction of gas flow, but it is obvious along the direction vertical to gas flow.

J. Yu · Y. Wang (✉)
School of Mechanical Engineering, Key Laboratory for Power Machinery and Engineering of Ministry of Education,
Shanghai Jiao Tong University,
800 Dong Chuan Rd.,
Shanghai 200240, People's Republic of China
e-mail: ferretyu801@yahoo.com.cn

X. Cao
School of Mechanics and Civil Engineering,
China University of Mining and Technology,
11 Lu Ding Rd.,
Beijing 100083, People's Republic of China

X. Cao
School of Engineering, Shijiazhuang University of Economic,
136 East Huai An Rd.,
Shijiazhuang 050031, People's Republic of China

Keywords Solid oxide fuel cell · Coal gasification · Syngas · Performance

Introduction

China, as one of the countries that depend on coal, produces and consumes 42% of world coal energy. The conventional methods of coal utilization are confronted with the problems of low energy efficiency, heavy pollution, and so on. Many researchers have found that the economic loss caused by air pollution takes 3–7% of China's GDP. Among the pollution, about 70% of dust and carbon dioxide, 90% of sulfur dioxide, and 67% of NO_X come from burnt coal. Therefore, coal should be used more efficiently and cleanly in the future. Integrated gasification fuel cell (IGFC) hybrid power generation system is the optimal method of coal utilization [1]. In IGFC system, the impurities in coal are further removed and reused as resource such as sulfur [2]. Moreover, high purity carbon dioxide can be captured. IGFC system is combined with fuel cell, gas turbine, and steam turbine. Thus, its electric efficiency is over 60%. For high efficiency, large specific power, and good performance under off-design conditions, IGFC is considered as a promising system in which coal is to be utilized efficiently and cleanly [3].

Coal gasification converts solid coal into gaseous fuel, which is the mixture of CO, H_2, CO_2, H_2O, CH_4, and N_2. Oxygen blown gasification is typically used because less coal is needed to heat the reactants to the temperature required for gasification (600–1,700 K) [4]. Three types of coal gasification systems have been used through industry (moving bed, fluidized bed, and entrained flow). The technology of coal gasification is mature. However, the huge cost and energy consumption restrict the process of

commercialization. Nevertheless, the high electrical efficiency of fuel cell makes up these shortcomings.

Compared with other types of fuel cell, solid oxide fuel cells (SOFCs) have great advantages as the energy conversion device in IGFC system for higher energy efficiency, lower noise, less pollutant emission, and more fuel flexibility, in addition to their excellent electrical generation efficiency, system simplicity, and long-term stability for possible stationary and mobile applications [5]. Furthermore, SOFCs can directly reform hydrocarbon in the anode under its high-temperature working conditions [6, 7].

Many authors carried on the research of SOFC with syngas as fuel. K. Sasaki et al. [4] estimated the SOFC performance with the fuel of syngas by studying the current–voltage characteristics under different ratios of H_2 and CO. The results show that the bigger molar fraction of H_2 between H_2 and CO applied as fuel was, the better output voltage was obtained under the same working conditions. The research also tested the carrier gases of He, N_2, and Ar. The biggest output voltage was obtained when He was the carrier gas. The resistance increased with promoting temperature, especially in H_2 high rich syngas.

Furthermore, many trace species in coal affect the performance of SOFC. O.A. Marina et al. [8] found the formation of a series of bulk nickel phosphide phases in anode which eventually affected electronic percolation through the anode support. Moreover, cell performance losses were observed well before the entire anode was converted to bulk nickel phosphide. J.P. Trembly et al. [9] found that Be, Cr, K, Na, V, and Z trace species will form condensed phases and should not affect SOFC anode performance.

In previous work, the materials of electrode and electrolyte and the novel structures of planar SOFC were developed, and the computational models were validated by the experiment with hydrogen and methane as fuel [6, 10–13]. Also, the optimization and simulation of gasifier for poly-generation system was conducted [14]. Compared with previous modeling of SOFC, the fully three-dimensional models are used in this work. The coupled heat transfer of solid and fluid in porous media is considered. Moreover, the credible data of heat transfer, diffusion, and viscous are from the experiments and literature [15]. In addition, the gas diffusion in porous media is taken into account instead of the simple concentration overpotential. Furthermore, the relating chemical reaction model in this work is the effective kinetic model from experiments which were carried on by Central Research Institute of Electric Power Industry (CRIEPI) [10].

In this work, based on the commercial CFD software (CFX4.4) and the developed materials, structures, and mathematical models by our team, a fully three-dimensional mathematical model for planar SOFC using syngas as fuel has been constructed to investigate the performances of planar SOFC for IGFC hybrid power generation system. So, the more detailed spatial distributions of temperature, chemical species, local overpotential, electric potential, and current were obtained. These results were expected to be helpful for developing the IGFC system.

Computational model

After cleaning process, syngas flows into SOFC stacks to generate the power. In fact, SOFC stacks are made up of a series of single fuel cell, and each of them is connected by two others. Therefore, it is possible, and very likely, that most of single planar SOFC work under the same conditions. So the performance of SOFC stacks can be obtained through periodically analyzing the single fuel cell [12]. In SOFC cell, heat and mass transfer are coupled with each other.

The three-dimensional Navier–Stokes equations are taken into account for conservation of mass, momentum, and energy [16]. Although the flow in porous medium is mainly the laminar flow, the turbulent flow in gas passages should be considered, especially in air flow passages. The effect of turbulence is represented by the k–ε model [12].

In porous media, porosity and permeability should be considered. Thus, both Navier–Stokes equations and Darcy's law are used in the model of heat/mass transfer. In porous media, mass transfer, molecular diffusion, and Knudsen diffusion must be simultaneously processed [12, 17, 18]. In addition, the effective thermal conductivity in the porous medium can be computed as the volume average of the fluid conductivity and the solid conductivity [17, 19].

Electrochemical model

In SOFC, electrochemical reactions occur in three-phase-boundary layers of anode and cathode. In anode, the fuel (syngas) consists of H_2, H_2O, CH_4, CO, and CO_2, and in cathode, the oxidizer (air) is modeled as an O_2/N_2 mixture. According to the literatures, only in case of operating on pure CO, CO must be oxidized in an electrochemical reaction at the anode. Otherwise, a sufficient amount of hydrogen from the supplied fuel and the shift reaction is available as the reactant in the electrochemical model [20]. Therefore, hydrogen and oxygen are considered as the reactants of electrochemical reaction.

Table 1 Reaction equation and equilibrium constants

I	Reaction	$K_{eq,i}$	Dimensions
1	$CH_4+H_2O\rightleftarrows CO+3H_2$	1.198×10^{17} exp (−26,830/T)	kPa^2
2	$CO+H_2O\rightleftarrows CO_2+H_2$	1.767×10^{-2} exp (4,400/T)	kPa^0
3	$CH_4+2H_2O\rightleftarrows CO_2+4H_2$	2.117×10^{15} exp (−22,430/T)	kPa^2
4	$CH_4+CO_2\rightleftarrows 2CO+2H_2$	6.780×10^{18} exp (−31,230/T)	kPa^2
5	$CH_4+3CO_2\rightleftarrows 4CO+2H_2O$	2.170×10^{22} exp (−40,030/T)	kPa^2
6	$CH_4\rightleftarrows C+2H_2$	4.161×10^{7} exp (−10,614/T)	kPa
7	$2CO\rightleftarrows C+CO_2$	5.744×10^{-12} exp (20,634/T)	kPa^{-1}
8	$CO+H_2\rightleftarrows C+H_2O$	3.173×10^{-10} exp (16,318/T)	kPa^{-1}
9	$CO_2+2H_2\rightleftarrows C+2H_2O$	1.753×10^{-8} exp (12,002/T)	kPa^{-1}
10	$CH_4+2CO\rightleftarrows 3\ C+2H_2O$	4.190×10^{-12} exp (22,022/T)	kPa^{-1}
11	$CH_4+CO_2\rightleftarrows 2\ C+2H_2O$	0.730 exp (1,388/T)	kPa^0

The electrochemical reaction occurring at the interface of cathode/electrolyte is

$$O_2 + 4e^- \rightarrow 2O^{2-} \quad (1)$$

Then, the oxygen ion is transported through the electrolyte and into the active anode. The electrochemical reaction occurring at the interface of anode/electrolyte is

$$H_2 + O^{2-} \rightarrow H_2O + 2e^- \quad (2)$$

By the oxidation of H_2, the local electromotive force yielded is obtained, which is affected by the gas composition and temperature. In the calculation, the local electromotive can be determined by the well-known Nernst equation [21].

$$E_{TPB} = \frac{-\Delta G}{2F} = \frac{-\Delta G^o}{2F} + \frac{RT}{2F}\ln\left(\frac{P_{H_2,TPB}P^{0.5}_{O_2,TPB}}{P_{H_2O,TPB}}\right) \quad (3)$$

In the equation, ΔG is Gibb's free energy at temperature T. F and R are Faraday constant and gas constant. P is the pressure.

In SOFC cell, the main losses are the concentration overpotential, the activation overpotential, and the ohmic overpotential. When the current density is high and the fuel concentration is small ($U_f \geq 80\%$), the concentration overpotential becomes an important loss.

Table 2 Physical properties of fuel cell components

Geometry parameters	
Length (m)	80×10^{-3}
Width (m)	80×10^{-3}
Anode three-phase layer thickness (m)	1×10^{-3}
Cathode three-phase layer thickness (m)	0.05×10^{-3}
Electrolyte thickness (m)	0.03×10^{-3}
Inter-connector thickness (m)	0.5×10^{-3}
Width × height of passages in electrode (m m)	$4\times10^{-3}\times2\times10^{-3}$
Material properties	
Thermal conductivity of anode ($Wm^{-1}\ K^{-1}$)	6.23
Thermal conductivity of cathode ($Wm^{-1}\ K^{-1}$)	9.6
Thermal conductivity of electrolyte ($Wm^{-1}\ K^{-1}$)	2.7
Thermal conductivity of inter-connector ($Wm^{-1}\ K^{-1}$)	9.6
Electric resistivity of anode (Ωm)	2.98×10^{-5} exp (−1,392/T) [14, 15]
Electric resistivity of cathode (Ωm)	8.11×10^{-5} exp (600/T) [14, 15]
Ionic resistivity of electrolyte (Ωm)	2.94×10^{-5} exp (10,350/T) [14, 15]
Electric resistivity of inter-connector (Ωm)	6.41×10^{-8} [14, 15]
Porosity of anode	0.38
Porosity of cathode	0.5

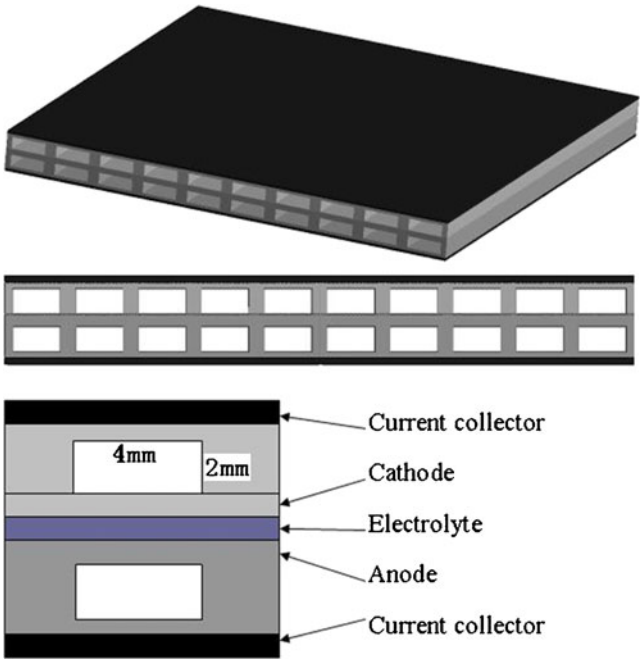

Fig. 1 Schematic view of planar electrode-supported SOFC

On the other hand, the ohmic overpotential is determined by the current density and the electric/ionic resistivity of the cell component materials which have the relationship with the temperature.

Near the electrolyte layer, the oxygen ions transfer to the anode from the cathode and react with hydrogen to form water. In this process, the activation overpotential must be overcome. Thus, the localized ionic transfer rate through the electrolyte layer can be obtained.

$$i = \frac{E_{\mathrm{TPB}} - \eta^{\mathrm{act}} - (V^{\mathrm{c}} - V^{\mathrm{a}})}{R^{\mathrm{e}}_{\mathrm{Ohm}}} \tag{4}$$

Activation overpotential

When the electrochemical reaction occurs, the activation overpotential must be overcome by the reacting species. The activation overpotential is controlled by the electrode kinetics at the electrode surfaces and occurred at both anode and cathode. With the increasing of the operating temperature, the electrode reaction enhances; thus, the activation overpotential usually reduces. However, as the operating temperature falls, it can become the most significant cause of voltage drop. It is often represented by the non-linear Butler–Volmer equation, which relates the current density drawn to the activation overpotential and, for a first order charge transfer controlled electrochemical reaction, is given by:

$$\frac{j}{j_0} = \exp\left(\alpha \frac{zF\eta^{\mathrm{act}}}{RT}\right) - \exp\left(-(1.0-\alpha)\frac{zF\eta^{\mathrm{act}}}{RT}\right) \tag{5}$$

where j_0 is the exchange current density, given by [18]:

$$j_0^{\mathrm{a}} = 5.5 \times 10^8 \left(\frac{P_{\mathrm{H_2}}}{P_{\mathrm{Ref}}}\right)\left(\frac{P_{\mathrm{H_2O}}}{P_{\mathrm{Ref}}}\right) \times \exp\left(\frac{-100 \times 10^3}{RT}\right) \tag{6}$$

$$j_0^{\mathrm{c}} = 7.0 \times 10^8 \left(\frac{P_{\mathrm{O_2}}}{P_{\mathrm{Ref}}}\right)^{0.25} \times \exp\left(\frac{-120 \times 10^3}{RT}\right) \tag{7}$$

The Butler–Volmer equation is solved numerically in this work. The most commonly used method for solving non-linear equations is the Newton–Raphson method.

Chemical reactions in anode

Syngas from coal gasification includes H_2, CO, H_2O, CO_2, and CH_4. The overall chemical reactions in anode may be presented by the equations listed in Table 1 [22]. Indeed, CO_2 reforming (reactions 4 and 5) is a linear combination of methane steam reforming reaction (reactions 1 and 3) and water shift reaction (reaction 2). The rates of reactions 4, 5, and 9–11 could be quite slow in terms of thermodynamics. Therefore, they are not considered to occur from the viewpoint of kinetic analysis [22]. Because the molar fraction of methane in syngas is low, the effect of methane is ignored. Thus, water shift reaction is considered to be dominant.

Table 3 Operating conditions

Operating pressure (Pa)	1.013×10^5
Inlet temperature (K)	1,273.15
Inlet flow rate of air (kg s^{-1})	4.30×10^{-5}
Inlet flow rate of syngas (kg s^{-1})	4.58×10^{-6}
Averaged current density (A m^{-2})	4,000
Electrochemical reaction area (m^2)	6.4×10^{-3}
Fuel efficiency (%)	80

Table 4 Composition of syngas

Composition	Molar fraction (%)
CO	39.58
H_2	30.28
CO_2	10.78
H_2O	16.45
CH_4	0.079

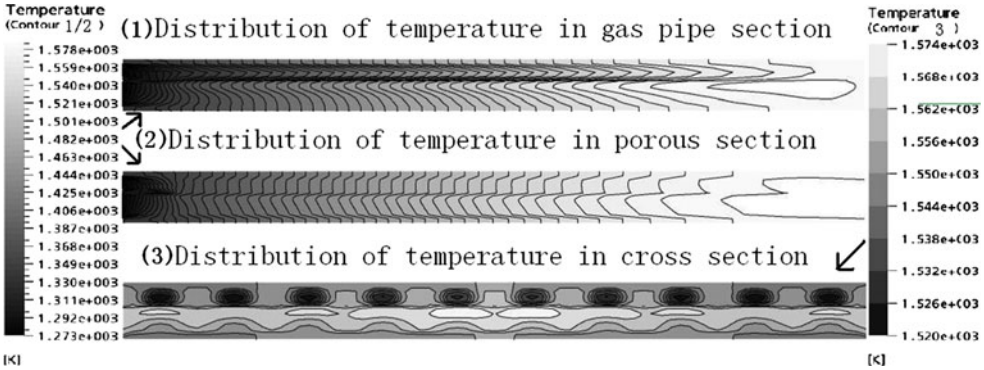

Fig. 2 Distribution of temperature in SOFC

Validation of the model

The materials of SOFC are Ni–YSZ/YSZ/LSM which were developed in previous work. The measured physical properties of the cell components are listed in Table 2. With these materials, the performance of the prototype SOFC cell using hydrogen as fuel was investigated by experiments and numerical analysis [12]. The numerical computational results agree with the experimental data. That is to say, the models of electrochemical/chemical, gas diffusion, heat, viscosity, etc. used in this numerical analysis are correct and reliable. Also, the performance of methane steam reforming over this Ni/YSZ porous anode was studied, and the effective kinetic models over this Ni/YSZ porous anode was developed by our team, under heat/mass transfer and species diffusion limitation [10]. In the anode, the syngas mainly consist of H_2, CO, H_2O, CO_2, and CH_4, and it is similar with the gas compositions when the cell uses natural gas as fuel. Therefore, the above reliable mathematical models can be used to investigate the performance of planar SOFC cell using syngas as fuel, and the detailed introduction of these models is given in [10, 12].

In this work, the numerical analysis is performed with the following assumptions:

1. The simulation is based on steady state.
2. Radiative heat transfer is ignored in the porous media.
3. Most of single fuel cells are working under the same conditions in the stack. The outside surfaces of two inter-connectors are specified to the periodic boundary.
4. The inlet of cathode and anode is set to the mass flow inlet, and the outlet is set to the pressure outlet.
5. Fuel and air run in co-flow.

Results and discussion

The structured grid is generated with 30 grids in length, 40 grids in width, and 19 grids in thickness. And the calculating accuracy is 1.0×10^{-6}.

Figure 1 shows the schematic view of planar electrode-supported SOFC. The cell size designed by our team and the physical properties of the cell components measured by

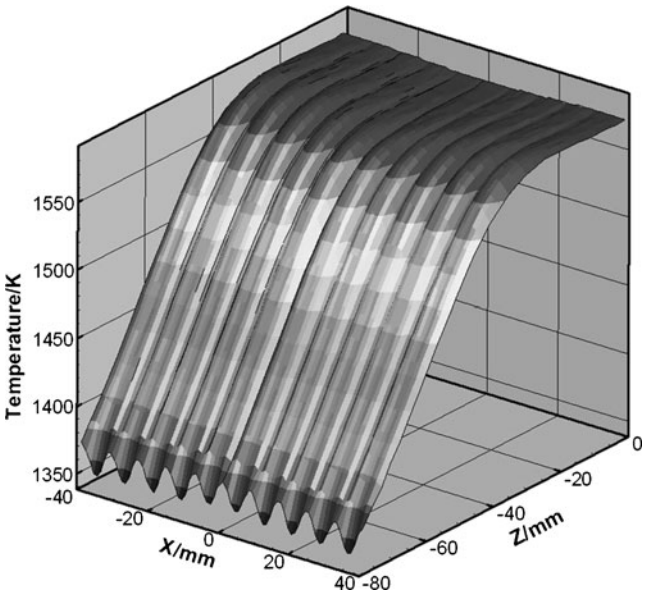

Fig. 3 Distribution of temperature in electrolyte of SOFC

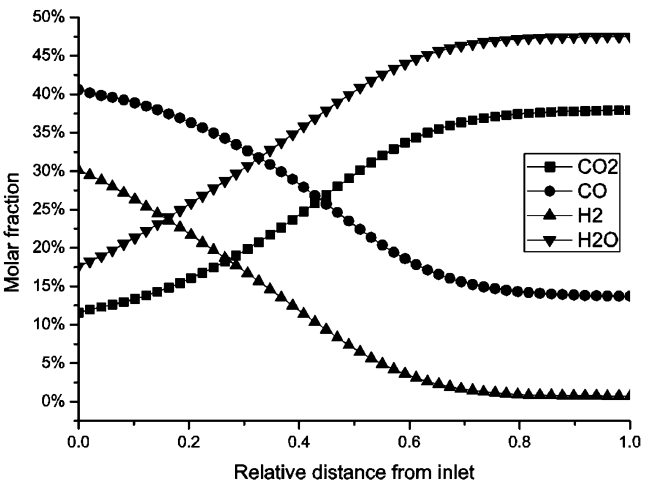

Fig. 4 Distribution of species along the flow direction in anode

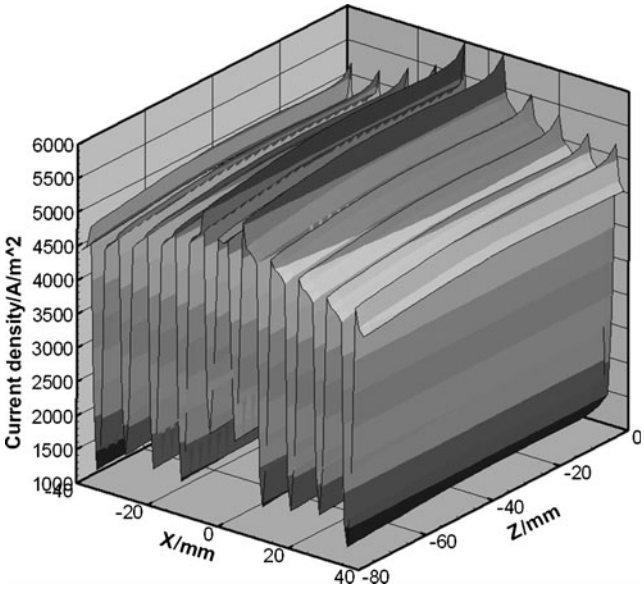

Fig. 5 Distribution of current density in the electrolyte layer

CRIEPI of Japan [12] are list in Table 2. The calculation conditions and the composition of syngas are listed in Tables 3 and 4, respectively. The syngas is from Texaco Gasifier and the coal type is Illinois 6. Meanwhile, the trace species are ignored in this work [14, 23]. According to the performance of the cell using the same materials when the cell is fed with hydrogen [12], the power density is the highest when the current density is 4,000 A m^{-2}. Therefore, in this work, the current density is also chosen as 4,000 A m^{-2}.

Distribution of temperature

According to the relationship between temperature and electric/ionic resistance of electrode/electrolyte, the ohmic overpotential reduces with the increasing temperature of SOFC, as shown in Table 2. Considering the thermal impact on the ceramic materials, the temperature gradient in SOFC should be controlled within a reasonable range. At the same time, the problem of sealing SOFC stacks occurs for different expanding ratios of electrode, electrolyte, and current collecting layers when the temperature is too high. Therefore, it is necessary to investigate the temperature distribution of SOFC to provide the optimal design of SOFC and the choice of fuel.

Figure 2 shows the distribution of temperature in SOFC along the flow direction and in cross section. At the co-flow, the heat from electrochemical reaction makes the temperature increase. Thus, with gas flowing, the temperature increases gradually. And, the highest temperature area is near the outlet region of anode in SOFC.

At the same distance from the inlet, the temperature in anode is higher than that in cathode, especially in gas passage region. The heat released from electrochemical reaction in the three-phase boundary layer is transferred to anode and cathode. At the same time, water shift reaction in anode also releases heat. In porous media, the flow rate is rather small; thus, heat conduction is dominant. So temperature in anode is higher than that in cathode. In gas passage, turbulent flow is dominant, and the mass flow rate of air is bigger than that of fuel in anode. Thus, the temperature in cathode is lower than that in anode obviously at the same distance from inlet. From the cross section of SOFC, the lower temperature near the flow passages and the higher temperature in the porous media make a large temperature gradient in this direction, and it is bad for SOFC.

Figure 3 shows the distribution of temperature in the electrolyte layer. Compared with the cathode and anode, the ohmic overpotential in electrolyte is larger and sensitive to temperature. In this work, the thickness of the electrolyte layer is 30 μm and easily breaks for big temperature gradient. So it is important to analyze the temperature distribution in electrolyte layer. With gas flowing, the temperature increases and the slope coefficient decreases a little near the outlet. The reason may be that the average rate of electrochemical reaction along the gas flow direction changes little which can be proved by the distribution of current density. Thus, the heat released from electrochemical reaction is similar along the gas flow. However, the temperature of inlet gas is relatively low; thus, the max temperature gradient is formed near the gas inlet. With the gas flowing, the heat is transferred sufficiently, and the temperature gradient reduces as well.

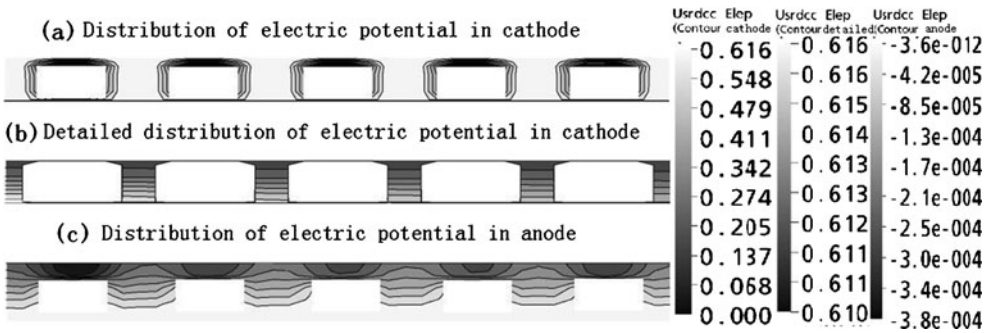

Fig. 6 Distribution of electric potential in porous electrode region

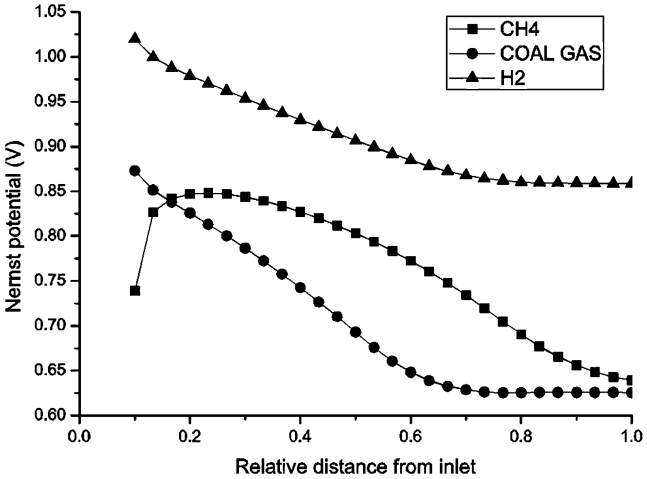

Fig. 7 Comparison of Nernst potential of SOFC among the fuels of hydrogen/syngas/natural gas under the same working conditions (current density is 4,000 A m^{-2})

Distribution of species

With the different relationships between reaction equilibrium constants and temperature, the molar fractions of species change differently as well. As Fig. 4 shows, CO joins in the electrochemical reaction and water shift reaction as well. So the molar fraction of CO is decreasing gradually and CO_2 is increasing by about 26.3% according to these two reactions under the working conditions. In the outlet region, hydrogen is nearly exhausted and the molar fraction of CO decreases by about 25%. Thus, the outlet gas in anode contains little hydrogen, 13.7% carbon monoxide, 37.9% carbon dioxide, and 47.5% water steam.

The reactant is air in cathode. The main functions of air are supplying the oxidant and cooling the fuel cell. Therefore, comparing the quantity of fuel gas, the air is excessive. Thus, the decrement of oxygen is inconspicuous (less than 4% in molar fraction).

Distribution of current density

The distribution of current density in electrolyte layer is affected by complex factors such as concentration overpotential, activation polarization, ohmic overpotential, structure of fuel cell, and so on. Figure 5 shows the distribution of current density in electrolyte layer. In *X* direction, the current density varies sharply. One of the reasons may be that the current must be conducted in the solid, and it should go across the gas passage. Thus, the variation of current distribution is enhanced. In the slice of flow passages, the concentration overpotential is lower than that in porous media for shorter way of diffusion. And at the same time, the temperature in flow passage region is lower than that in porous region seen above. This results in the higher activation overpotential and ohmic overpotential. Moreover, the current must conduct in the solid electric material and go across the gas passage region; thus, the gas passage enhances the variation of current density. So the better choices of the porosity of electrode and the size of gas passage benefit the diffusion of gas species and enhance the performance of SOFC.

Along the direction of gas flowing, the variation of average current density is unobvious (less than 2.5%). The average current density increases a little with the gas flowing. The main reason may be that the ohmic overpotential reduces with the temperature increasing. Near the outlet of the cell, the temperature reaches the maximum value, and at the same time, the current density is the largest.

Distribution of electric potential

The distributions of electric potential of SOFC are shown in Fig. 6. Figure 6a shows the overall distribution of electric potential in cathode. The variation of electric potential in the middle part of porous media is rather small. And near the wall of gas passage, the difference of electric potential is obvious. Figure 6b shows the detailed change of electric potential in the middle part of porous medium in cathode. And the change is less than millesimal. Figure 6c shows the change of electric potential in the anode. Compared with that in the cathode, the change of electric potential near the wall of gas passage in the anode is unobvious. The current flowing into and out of the electrolyte layer will go across the flow passage. The distance between the bulk flow and the electrolyte layer in the anode is longer than that in the cathode; thus, the current is easier to go across the gas passage in the anode. So the change of electric potential in the anode is more unobvious than that in the cathode. Therefore, when designing the structure of SOFC, the optimal size of gas passage and thickness of electrode should be considered to enhance the gas diffusion and lower the ohmic overpotential.

Comparing with that using hydrogen and natural gas (CH_4) as fuel, the distribution of Nernst potential of the same SOFC is different using syngas as fuel. In Fig. 7, under the same working conditions, the biggest Nernst potential is obtained by the SOFC with hydrogen as fuel. The area-averaged Nernst potentials of SOFC with natural gas and syngas as fuel are 0.763 and 0.704 V, respectively. Near the inlet, Nernst potential with syngas as fuel is higher than that with natural gas as fuel. But in the middle of fuel cell, the result is opposite. The reason may be that H_2 and CO in syngas can directly join the electrochemical reaction. And simultaneously, abundant hydrogen is supplied by water shift reaction and methane steam reforming reaction. So the reactant of electrochemical reaction is enough. However, the hydrogen in SOFC with natural gas as fuel is supplied by methane steam reforming reaction which is strong endothermic reaction. For lack of hydrogen, the Nernst potential in SOFC

with natural gas as fuel is smaller than that in SOFC with syngas as fuel near the inlet. But in the middle section, the abundant hydrogen is supplied and the Nernst potential with natural gas as fuel is higher than that with syngas as fuel in which hydrogen is almost exhausted.

Conclusion

In this work, the performance of planar electrode-supported SOFC with syngas as fuel was investigated. The distributions of temperature, species, current density, and electric potential were analyzed. The conclusions are as follows:

1. Under the calculation conditions in this work, the max temperature gradient is formed near the gas inlet section, and the temperature gradient reduces along the gas flowing direction.
2. As the equilibrium constant of water gas shift reaction reduces with the temperature increasing, the decrement of molar fraction of hydrogen is larger than that of carbon monoxide with the reactions processing under the calculation conditions.
3. The concentration overpotentials in porous medium and the size of gas passage strongly affect the distribution of current density in electrolyte layer. So it is important to choose an optimal porosity and size of gas passage.
4. In this work, under the calculation conditions, the Nernst potential of SOFC with syngas as fuel is lower than that with hydrogen as fuel, but similar with that using natural gas as fuel.

Nomenclature

E_{TPB}	Electromotive force (V)
F	Faraday's constant, 96,487 (C mol^{-1})
i	Current (A)
j	Current density (A m^{-2})
j_0	Exchange current (A m^{-2})
P	Pressure (Pa)
$P_{i,\mathrm{TPB}}$	The ratios of partial pressure over the standard state pressure of 1.013×10^5 Pa at the electrolyte/electrode interface $i \in \{H_2, H_2O, O_2\}$
R	Universal gas constant (J kg^{-1} K^{-1})
R_{ohm}	Ohm resistance (Ω)
T	Temperature (K)
U_{f}	Fuel utilization factor
V^{c},V^{a}	Electrical potential at anode and cathode, respectively (V)
z	Number of electrons

Greek symbols

α	Electron transfer coefficient (usually taken to be 0.5)
κ	Turbulent kinetic energy (m^2 s^{-2})
ε	Turbulent dissipation rate (m^2 s^{-3})
η^{act}	Overpotential incurred by the activation polarization (V)

Subscripts

Ref Reference

Superscripts

a Anode
c Cathode
e Electrolyte

Acknowledgments This work was supported by the Scientific Research Foundation for Returned Scholars, Ministry of Education of China, Shanghai Jiao Tong University Innovation Fund For Postgraduates, National Basic Research Program of China (2007CB210102), and Key Technologies R & D Program of Shanghai (08DZ1200102).

References

1. Li M, Rao AD, Brouwer J, Samuelsen GS (2010) Design of highly efficient coal-based integrated gasification fuel cell power plants. J Power Sources 195:5707–5718
2. Hepworth MT, Bender FN (1996) Recovery of lime and sulfur products from utility coal wastes. J resource management and technology 23:1–7
3. Eric G (2009) Technical assessment of an integrated gasification fuel cell combined cycle with carbon capture. Energy Procedia 1:4307–4334
4. Sasaki K, Hori Y, Kikuchi R, Eguchi K, Ueno A, Takeuchi H, Aizawa M, Tsujimoto K, Tajiri H, Nishikawa H, Uchidad Y (2002) Current–voltage characteristics and impedance analysis of solid oxide fuel cells for mixed H_2 and CO gases. J The Electrochemical Society 149:A227–A233
5. Robert JK, Zhu HY, David G (2005) Solid-oxide fuel cells with hydrocarbon fuels. Proc the Combustion Institute 30:2379–2404
6. Yu JG, Wang YZ, Xu L, Weng SL (2009) Development and investigation on the steady state of Solid oxide fuel cell and hybrid power system. In: Proceedings of the 1st International Conference on Sustainable Power Generation and Supply, China
7. Peters R, Dahl R, Klüttgen U, Palm C, Stolten D (2002) Internal reforming of methane in solid oxide fuel cell systems. J Power Sources 106:238–244
8. Marina OA, Coyle CA, Thomsen EC, Edwards DJ, Coffey GW, Pederson LR (2010) Degradation mechanisms of SOFC anodes in coal gas containing phosphorus. Solid State Ionics 181:430–440
9. Trembly JP, Gemmen RS, Bayless DJ (2007) The effect of IGFC warm gas cleanup system conditions on the gas–solid partitioning and form of trace species in coal syngas and their interactions with SOFC anodes. J Power Sources 163:986–996
10. Wang YZ, Yoshiba F, Kawase M, Watanabe T (2009) Performance and effective kinetic models of methane steam reforming over Ni/YSZ anode of planar SOFC. Int J Hydrogen Energy 34:3885–3893
11. Yu JG, Wang YZ, Hui Y, Weng SL (2009) The effect of anode porosity on the performance of planar electrode supported solid

oxide fuel cell. In: Proceedings of ASME 2009 2nd Micro/Nanoscale Heat & Mass Transfer International Conference, China
12. Wang YZ, Yoshiba F, Watanabe T, Weng SL (2007) Numerical analysis of electrochemical characteristics and heat/species transport for planar porous-electrode-supported SOFC. J of Power Sources 170:101–110
13. Wang YZ, Yoshiba F, Watanabe T (2006) Performance analysis of planar porous-electrode-supported SOFC. In: Proceedings of the International Conference on Clean Coal Technology and Fuel Cells, Yokosuka, Japan
14. Xu L, Wang YZ, Weng YW, Weng SL (2009) Simulation and optimization on gasifier in the poly-generation system with IGCC. In: Proceedings of the International Conference on Clean Coal Technology and Fuel Cells, Daejoen, Korea
15. Todd B, Young JB (2002) Thermodynamic and transport properties of gases for use in solid oxide fuel modeling. J Power Sources 110:186–200
16. Wang YZ, Li YX, Weng SL, Wang Y (2007) Numerical simulation of counter-flow spray saturator for humid air turbine cycle. Energy 32:852–860
17. Chan SH, Khor KA, Xia ZT (2001) A complete polarization model of a solid oxide fuel cell and its sensitivity of the change of cell component thickness. J Power Sources 93:130–140
18. Hwang JJ, Chen CK, Lai DY (2005) Computational analysis of species transport and electrochemical characteristics of a MOLB-type SOFC. J Power Sources 140:235–242
19. Bessette N (1994) Modeling and simulation for solid oxide fuel cell power systems. Doctorial thesis, Georgia Institute of Technology, Atlanta
20. Weber A, Sauer B, Müller AC, Herbstritt D, Ivers-Tiffée E (2002) Oxidation of H_2, CO and methane in SOFCs with Ni/YSZ-cermet anodes. Solid State Ionics 152:543–550
21. Costamagna P, Selimovic A, Del Borghi M, Agnew G (2004) Electrochemical model of the integrated planar solid oxide fuel cell (IP-SOFC). Chem Eng J 102:61–69
22. Hou K, Hughes R (2001) The kinetics of methane steam reforming over a Ni/α-Al2O catalyst. Chem Eng J 82:311–328
23. Simbeck DR, Korens N (1993) Coal gasification guidebook: status, applications and technologies. Electric Power Research Institute, USA